

Solar Rotation Effects in Earth's and Mars' Thermospheric Densities as Revealed by Concurrent MAVEN, Swarm-C, and GOES Observations

Federico Gasperini^{1*}, J. Hughes¹, and E. M. B. Thiemann²

¹Orion Space Solutions, Louisville, CO, USA

²Laboratory for Atmospheric and Space Physics, University of Colorado, Boulder, CO, USA

Key Points:

- Solar rotation effects are quantified in over 6 years of simultaneous Mars' and Earth's density and flux satellite observations
- Earth's middle thermospheric daytime density is 30-50% (10-30%) more responsive than Mars' during solar maximum (minimum) conditions
- Density sensitivities to the solar rotation in flux show prominent dependencies on altitude and solar flux at both planets

*282 Century Place, Suite 1000, Louisville, CO, 80027

Corresponding author: Federico Gasperini, federico.gasperini@orionspace.com

Abstract

The responses of Earth's and Mars' thermospheric densities to quasi-periodic (~ 27 -day) solar rotation variations in flux were measured contemporaneously by the Mars Atmosphere and Volatile Evolution (MAVEN), Geostationary Operational Environmental Satellites (GOES), and Swarm-C satellites. While large solar rotation variability is found in both planetary thermospheres, correlation analyses performed on over 6 years of observations reveal that, independently of flux level, Earth's daytime density response is about 10-50% larger than Mars' at a similar density level. Important altitude dependencies in the density sensitivity to the solar rotation in flux are found in the Martian thermosphere, while the terrestrial thermosphere is shown to exhibit only small ($\pm 5\%$) day/night and latitude variations in the response. Detailed analyses focused on correlative periods in 2015-2016 and 2020 indicate important solar cycle effects in the sensitivities of both planetary thermospheres, with increased slopes under low solar flux conditions. These results provide important new insights into processes relevant to the interpretation of the sources of short-term density variability in Mars' and Earth's thermospheres associated with solar drivers and point to the need for targeted modeling efforts along with dedicated data analyses to help resolve current unknowns in thermal balance processes.

Plain Language Summary

The quasi-periodic change in solar extreme ultraviolet (EUV) radiation from active regions on the Sun rotating with a period of about 27 days is one of the largest sources of short-term variability in the thermospheres of both Mars and Earth. This work investigates the response of total mass densities in the thermospheres of Mars and Earth to the solar rotation variation in flux, as a tracer of short-term solar-driven impacts on thermospheric densities, using simultaneous density and flux observations from the Mars Atmosphere and Volatile Evolution (MAVEN), Swarm-C, and Geostationary Operational Environmental Satellites (GOES) satellites from 2014 through 2021. Earth's daytime densities in the middle thermosphere are found to be about 10-50% more responsive than Mars' for an equivalent altitude. Important dependencies on height are found at Mars, while small day/night and latitude dependencies are found at Earth. Correlation analyses also suggest strong solar cycle effects in the sensitivities, with significantly higher sensitivities during solar minimum. The results of this study can help to better constrain comparative planetary thermosphere simulations and resolve unknowns in thermal balance processes but also suggests the need for additional data- and modeling-driven studies.

1 Introduction

The response of planetary upper atmospheres, including Earth and Mars, to variability in solar extreme ultraviolet (EUV) of critical importance in solar-planetary physics. The thermospheres of Earth and Mars share some similarities, yet are profoundly different, making their comparative study an excellent way to test the fidelity of models and theories across a broad range of parameters. Solar EUV heating and cooling by molecular thermal conduction, along with heating efficiency and dynamics, are critical to the response of both planetary thermospheres to solar radiation (e.g., Bougher et al., 2000, 2015; Forbes et al., 2008). Solar EUV (~ 10 -121 nm) radiation is the primary energy input to Mars' and Earth's thermospheres. For both planets, the most significant fraction of EUV irradiance is absorbed at altitudes ranging from about 100 km (i.e., $\sim 10^{-2}$ Pa for both Mars and Earth) and 220 km (i.e., $\sim 10^{-5}$ Pa for Earth and $\sim 10^{-8}$ Pa for Mars). Variability in EUV radiation spans significantly different time scales, from hours for solar flares and weeks for solar rotation to years for the solar cycle (e.g., Lean, 1997). Longer wavelengths tend to be less variable than shorter wavelengths as they are primarily originating in the solar chromospheric region instead of the more variable solar corona (Woods

et al., 2005, 2015; Thiemann et al., 2017a,b). Near the sub-solar regions, the peak absorption occurs near 130 km on Mars (i.e., $\sim 10^{-4}$ Pa; Bougher, 1995; Bougher et al., 2000, 2009, 2015; Gonzalez-Galindo et al., 2015; Thiemann et al., 2018) and 200 km on Earth (i.e., $\sim 10^{-4}$ Pa; Hedin and Mayr, 1987; Roble et al., 1987). Mars' thermosphere is primarily composed of carbon dioxide (CO_2), atomic oxygen (O), molecular nitrogen (N_2), carbon monoxide (CO), argon (Ar), molecular oxygen (O_2), and atomic nitrogen (N) (Bougher et al., 1995, 2009; Mahaffy et al., 2015; Zurek et al., 2017; Stone et al., 2018), while Earth's thermosphere is mainly composed by O, N_2 , O_2 , helium (He), and hydrogen (H) (Dickinson et al., 1981; Roble et al., 1987; Forbes, 2007). The rotation of active regions on the Sun produces periodicities in EUV radiation, the most prominent of which is near the mean rotation period of ~ 27 days (e.g., Fan 2009, 2021). This variability in EUV is subsequently absorbed by planetary thermospheres and generates thermospheric variability with time scales ranging from about 25 days to 35 days. Shorter-period EUV-driven thermospheric variability is also possible as a result of the absorption of flux variability at subharmonics of the main solar rotation variation. The EUV irradiance reaching Earth's and Mars' atmospheres have some notable differences (e.g., Thiemann et al., 2017, 2018): (1) at any given time the solar hemisphere visible from Mars may have more or less numerous or intense EUV source regions than the solar hemisphere visible from Earth, (2) irradiance at Mars is $\sim 36\text{-}53\%$ of that reaching Earth at 1 AU as irradiance falls off inversely with the square of the distance from the Sun, (3) planetary orbital eccentricity plays a larger role at Mars compared to Earth, with irradiance at Mars varying by about 40% over the course of the Martian year (e.g., Woods and Rottman, 2002; Bougher et al., 2017; Zurek et al., 2017).

Variability in Mars' thermospheric density is primarily generated by processes related to EUV flux absorption, molecular thermal conduction, CO_2 cooling, and adiabatic heating and cooling due to dynamics (Bougher et al., 1999, 2000, 2015, 2017; Forbes et al., 2006). Previous studies (e.g., Hagan and Oliver, 1985; Forbes et al., 2006) indicated the terrestrial response to EUV-driven circulation and adiabatic cooling is less prominent than Mars' due to the effect of ion drag. The resulting suppression of cooling leads to more heating from a given EUV increase, resulting in a stronger response to long-term changes in flux at Earth. Forbes et al. (2006) employed simultaneous density observations from the Challenging Minisatellite Payload (CHAMP) and Mars Global Surveyor (MGS) satellites to investigate Earth's and Mars' thermospheric responses to the solar rotation variation in flux using the F10.7 solar radio flux as a proxy for EUV and revealed a response that is twice as large for Earth than for Mars. Forbes et al. (2006) and related studies (e.g., Forbes et al., 2007; Keating and Bougher, 1987, 1992; Bougher et al., 1999; Thiemann and Dominique, 2021) established that exospheric temperatures at Mars are about 30-50% as responsive as Earth to the ~ 27 -day solar rotation variation in EUV. This different response is discussed to be mainly associated with larger damping of solar EUV energy at Mars due to increased CO_2 cooling. These results were more recently confirmed by Thiemann and Dominique (2021), who showed Mars' exospheric EUV temperature sensitivities to be about 0.47 times as sensitive to EUV variability as those at Earth.

In a recent study, Fang et al. (2022) investigated the relative contribution of local effects from EUV heating and indirect effects associated with solar infrared (and thus upward coupling from the middle atmosphere) to generate thermospheric density variability using Mars Atmosphere and Volatile Evolution (MAVEN) Neutral Gas and Ion Mass Spectrometer (NGIMS) data. These authors reported that the indirect effects from solar infrared decreased with altitude and the local EUV effect increased with altitude. In a related study, Hughes et al. (2022) investigated solar rotation effects on the Martian thermospheric density from ~ 125 km to ~ 250 km using over 5 years of concurrent MAVEN/NGIMS and MAVEN/EUV Monitor (EUVM) instruments. Large EUV-driven effects were found in CO_2 , Ar, and N_2 thermospheric densities, with effects increasing with altitude (up to $\sim 200\text{-}230$ km) and strong dependencies on the particular species and

flux band examined. The increase of sensitivities up to about 230 km was explained by the increasing energy per particle with altitude (similar to the terrestrial results in Thiemann et al., 2017a), while the decrease of sensitivities above about 230 km was ascribed to additional complexities potentially introduced by solar wind effects near or above the Martian exobase (e.g., Chaffin et al., 2015; Hughes et al., 2021).

This work seeks to reveal and quantify the contemporaneous response of the terrestrial and Martian thermospheric densities to solar rotation variability in flux using in situ density and flux observations from the MAVEN, Swarm-C, and Geostationary Operational Environmental Satellites (GOES) satellites from late 2014 during solar maximum through mid-2021 near solar minimum. This study presents detailed analyses of the comparative responses of Earth’s and Mars’ thermospheric densities to the solar rotation-related variability in EUV flux using simultaneous in situ irradiance and density measurements and further investigates altitude and solar cycle dependencies in these responses. These analyses represent a significant advancement over previous investigations (e.g., those noted above), being uniquely enabled by MAVEN’s orbital characteristics and recent solar minimum measurements (2018-2021) that allow for altitude-dependencies (~ 150 -230 km) and solar cycle effects to be resolved. After a brief description of the observational datasets (Section 2), Section 3 provides details on the data processing techniques, Section 4 contains results from the comparative and correlation analyses, while Section 5 discusses the main findings and summarizes the results.

2 MAVEN, Swarm-C, and GOES Observations

MAVEN is the second Scout-class spacecraft mission to Mars selected by NASA (Jakosky et al., 2015). MAVEN entered Mars’ orbit on 21 September 2014 and, after a two-month transition phase, reached its nominal science elliptical orbit, with 75° inclination, a ~ 4.5 -hr period, apoapsis near 6200 km, and periapsis near 140-160 km, determined by a targeted density corridor of 0.05 to 0.15 kg km $^{-3}$. MAVEN’s periapsis samples five to six longitudes around the planet every Mars day (sol) and precesses through ~ 3.5 diurnal cycles every Mars year. On 5 April 2019, MAVEN completed a two-month aerobraking maneuver and was temporarily lowered to an elliptic orbit of $\sim 4,500$ km by ~ 130 km and ~ 6.6 orbits to better serve as a communications relay. Starting in August 2020, MAVEN was placed in a more fuel-efficient and stable orbit with periapsis near ~ 180 -220 km. MAVEN’s instruments include the NGIMS designed to measure atmospheric densities at altitudes below about 500 km (Mahaffy et al., 2014, 2015) and the EUVM measuring solar irradiance in the 0.1-7 nm, 17-22 nm, and 117-125 nm bands selected to characterize EUV emissions from distinctly different regions of the solar atmosphere (Epavier et al., 2015). The altitude profiles of CO $_2$, N $_2$, O, Ar, CO number densities that are continuously measured by NGIMS from ~ 150 km to ~ 200 -230 km have been used in several thermospheric studies (e.g., England et al., 2016, 2017, 2019; Liu et al., 2017; Terada et al., 2017; Yiğit et al., 2015; Hughes et al., 2022; Fang et al., 2022). EUVM measures solar irradiance continuously except when MAVEN is in eclipse or when both MAVEN is below 500 km and the Sun is in the direction of spacecraft motion, with an approximate solar measurement duty cycle of $\sim 60\%$. EUVM Level 3 (L3) irradiance data is processed using the Flare Irradiance Spectral Model for Mars (FISM-M) (Thiemann et al., 2016, 2017), which is an iteration of the FISM model of the FISM model of Chamberlain et al. (2007, 2008) for spectral irradiance at Earth. Away from solar flares, the relative uncertainty in the EUVM L3 daily averaged irradiance is generally less than $\sim 5\%$ for most wavelength bins, and the larger total uncertainty is mostly driven by the uncertainty in the data sets used for calibration (Thiemann et al., 2017).

Swarm constitutes the fifth Earth Explorer mission from the European Space Agency (ESA)’s Living Planet Programme (Friis-Christensen et al., 2008). Swarm is a constellation of 3 identical satellites (A, B, and C) that launched on 22 November 2013 into 87.4° inclination near-polar circular orbits. Swarm-B was placed in a relatively high orbit with

an average altitude of about 530 km, while the other two satellites were placed to fly almost side-by-side at a lower altitude of about 480 km (Van Den Lijssels et al., 2016). Swarm-A and -C nodes precess through 24 hours of local solar time (LT) in about 266 days. A Global Positioning System (GPS) receiver is used for the Precise Orbit Determination (POD) of the satellite, with a laser retroreflector that allowed validation of the orbits computed from the GPS observations (Siemes et al. 2016). Each Swarm satellite payload includes an accelerometer instrument to measure non-conservative forces (e.g., atmospheric drag, solar radiation pressure), which can be used to derive atmospheric mass density estimates (Visser et al., 2013; Yuan et al. (2019)). Due to significant data gaps in the accelerometer-based density retrievals, this work employs the temporally and spatially coarser POD-derived post-processed density product from Swarm-C. This POD-based product is considered more suitable than the accelerometer-based product for the type of investigation herein presented given the interest in large-scale variability with timescales greater than ~ 5 days. Comparisons with physical and empirical models and other satellite observations (e.g., Luo et al., 2022) indicate errors generally lower than 3% for the Swarm-C POD-based density retrievals.

The National Oceanic and Atmospheric Administration (NOAA) GOES satellites have monitored solar soft X-ray irradiance in two bands since their inception in 1975 with the X-Ray Sensor (XRS) instruments, while GOES 13-15 have measured EUV irradiance in several bands with the Extreme Ultraviolet Sensor (EUVS) instruments since 2006 (Viereck et al., 2007, Thiemann et al., 2019). For the GOES-R series satellites, new versions of the XRS and EUVS instruments have been built as part of the EUV and X-ray Irradiance Sensors (EXIS) instrument suite. The GOES-R series program is the latest iteration of the GOES satellite constellation and consists of 4 satellites, each carrying a suite of identical instruments designed to monitor terrestrial and space weather continuously. The GOES-R series satellites are named GOES 16-19 upon commissioning. GOES-16 was successfully launched on 19 November 2016. This study employs GOES-15 irradiance measurements near 121.6 nm from 28 November 2013 to 6 June 2016 and GOES-16 irradiance measurements near seven different flux bands from 25.6 nm to 140.5 nm from 10 February 2017 to 24 September 2021. While GOES-15 provides irradiance measurements near 121.6 nm only, GOES-16 detects seven different flux bands around 25.6 nm, 28.4 nm, 30.4 nm, 117.5 nm, 121.6 nm, 133.5 nm, and 140.5 nm. Thus, our analysis of GOES 121.6 nm contains a gap of 249 days between 6 June 2016 and 10 February 2017. Future work may explore the use of Solar Radiation and Climate Experiment (SORCE) SOLAR STellar Irradiance Comparison Experiment (SOLSTICE) (McClintock et al., 2005a,b; Snow et al., 2005) Lyman-alpha (Lyman- α) measurements (Machol et al., 2019) available from 14 April 2013 through 25 February 2020. Note that the inclusion of SORCE SOLSTICE data to cover this gap in GOES observations would not benefit the comparative nature of this investigation given the lack of statistically significant ($r > 0.5$) solar rotation variability in EUVM/NGIMS observations at Mars during this period.

3 Methods

NGIMS inbound verified (IV) CO₂, N₂, Ar, O and inbound unverified (IU) CO abundances are interpolated each orbit onto a 2.5 km resolution grid stretching from ~ 125 to ~ 275 km in altitude. We limit the analysis to inbound data to avoid possible contamination by heterogeneous chemistry as well as physical adsorption and desorption occurring on the instrument antechamber walls (Mahaffy et al., 2015). Analyses of IU CO (quality flag ‘0’) and the use of this dataset in previous studies (e.g., Girazian et al., 2019) demonstrate it to be suitable for the investigation herein conducted. Additionally, neglecting CO would lead to a significant underestimation of the total mass density at lower thermospheric altitudes, while including it can be assumed to be a minimum-error solution. Similar to Girazian et al. (2019), the abundance measurements are processed to

yield total mass density estimates by multiplying by the molecular mass, and adding the mass densities of CO₂, N₂, Ar, O, and CO. When N₂, Ar, O, or CO data are not available, their mass density contribution is assumed to be 0. If CO₂ data is not available, we avoid computing the mass density for that time and altitude. This method generates small non-physical jumps in the mass density as Ar, N₂, O, and CO data become available, but this effect is found to be small enough not to significantly impact the results. Note that MAVEN also produces periapsis density estimates using precise orbit determination (POD), but these data would not have enabled reliable density estimates at an altitude with a mean density equal to Swarm-C at Earth. Meanwhile, MAVEN accelerometer data at these altitudes are too noisy to provide reliable measurements of mass density. Similar to Hughes et al. (2022), EUVM L3 irradiance data are averaged in four spectral bands: 0-7 nm, 17-22 nm, 0-45 nm, and 117-125 nm. As noted by Thiemann et al. (2017), over ~90% of the signal measured by the 117-125 nm EUVM band lies in the 121-122 nm range thus, in the following, this band is referred to as the ‘Lyman- α ’, ‘121.6 nm band’, or ‘121.6 nm irradiance’.

Swarm-C POD-derived total mass densities and GOES irradiances are processed using methods similar to those detailed above. The time series of GOES 25.6 nm, 28.4 nm, 30.4 nm, 117.5 nm, 121.6 nm (scaled by a factor of 20), 133.5 nm, and 140.5 nm irradiances, Swarm-C mean altitude and LT, and total mass density from 28 November 2013 to 24 September 2021 are shown in Figures 1a-c. The Swarm-C densities in Figure 1c are obtained by combining ascending and descending node data (i.e., ‘proxies’ for daily zonal means, see e.g., Gasperini et al., 2015, 2020) and all latitudes ($\pm 87^\circ$). Distinct solar rotation variations near 27 days are present in the time series of all irradiances, particularly during solar maximum conditions in 2013-2016 and during 2017 and 2021. The Swarm-C mean altitude varies from about 500-530 km in early 2014 to ~430-460 km in 2021. The time series of in-situ-measured Swarm-C total mass density (Figure 1c) contains solar cycle variations, changes associated with the spacecraft’s lowering altitude, and periodicities around 133 days due to Swarm-C’s precession cycle. These longer-term (≥ 130 -day) variations are not contributing uncertainty to the correlation analysis techniques herein implemented given the data processing methods detailed below.

The time series of the 0-7 nm, 17-22 nm, 0-45 nm, and 121.6 nm (scaled by a factor of 5) EUVM irradiances, NGIMS altitude and LT, and NGIMS total mass density at ~220 km from January 2015 to May 2021 are shown in Figures 1d-f. The altitude of ~220 km is chosen to closely match the mean density level measured by Swarm-C during this time period. The four irradiances exhibit solar cycle, orbital eccentricity, and solar rotation variations largely reflected in the densities. The large variations with a period of about 200 days in the NGIMS total mass densities (Figure 1f) are largely due to MAVEN’s diurnal precession cycle. MAVEN’s inclination is $\sim 75^\circ$ thus all latitudes within about $\pm 75^\circ$ are sampled. Note also that MAVEN precesses through ~ 3.5 diurnal cycles every Martian year and that all latitudes within $\pm 75^\circ$ are sampled every ~ 400 days. Embedded in the densities are also prominent solar rotation variations that were examined in detail by Hughes et al. (2022) using statistical methods. Compared to Earth (cf., Figure 1a), Mars’ irradiances (Figure 1d) exhibit much larger orbital eccentricity effects due to the greater annual Sun-Mars distance change with solar longitude (Ls). These effects have been studied in detail by Fang et al. (2022) who investigated the relative contribution of orbital and EUV effects in thermospheric density variations and found that the solar EUV effect nearly monotonically increases with altitude while the orbital effect is relatively constant at low altitudes and then decreases with increasing altitude. The small (i.e., few-day) gaps in the NGIMS densities are not contributing significant uncertainty to the correlation analysis techniques given the interest in variations with solar rotation time scales (see below and Section 4 for further details).

To effectively quantify the density responses of Earth’s and Mars’ thermospheres to the solar rotation variation in flux, densities and irradiances are transformed into rel-

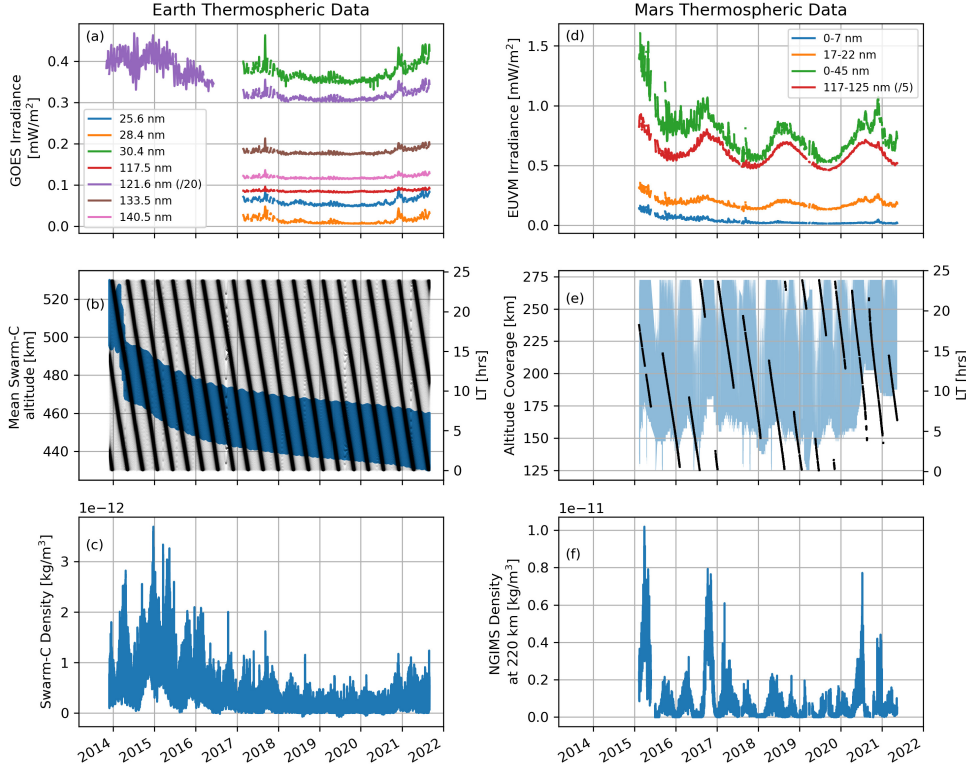


Figure 1. (a) Time series of GOES-15 121.6 nm irradiance (purple line, scaled by a factor of 20) from 28 November 2013 to 6 June 2016, and of GOES-16 25.6 nm (blue line), 28.4 nm (orange line), 30.4 nm (green line), 117.5 nm (red line), 121.6 nm (purple line, scaled by a factor of 20), 133.5 nm (brown line), and 140.5 nm (pink line) irradiances from 10 February 2017 until 24 September 2021. (b) Time series of Swarm-C mean altitude (blue lines, left y-axis) and LT (black line, right y-axis) from 28 November 2013 to 24 September 2021. (c) Time series of zonal mean Swarm-C POD-derived in situ total mass density during the same time interval as (b). A gap of 249 days between 6 June 2016 and 10 February 2017 is present where there are no 121.6 nm measurements from either GOES-15 or GOES-16. (d) Time series of EUVM 0-7 nm (blue line), 17-22 nm (orange line), 0-45 nm (green line), 121.6 nm (red line, scaled by a factor of 5) irradiances from January 2015 to May 2021. (e) MAVEN altitude coverage (blue lines, left y-axis) and local time (black line, right y-axis) for the same time interval as (d). (f) Time series of NGIMS total mass density for the same time interval as (d).

ative changes (e.g., Hughes et al., 2022; Gasperini et al., 2018). This treatment of the data is performed in four steps: (1) a uniform time vector with a one-day cadence is created spanning the entire dataset; (2) for each time in the uniform time vector the data within 20 days before or after (40 days total) are averaged to make x_{40} ; (3) for each time in the uniform time vector, the data within 2.5 days (5 days total) are averaged to make x_5 ; (4) the relative change is computed as $(x_5 - x_{40})/x_{40} \times 100\%$. This method is effective at isolating signals with periods between 5 and 40 days while removing higher- and lower-period variability. Relative change values computed using fewer than 30 days (i.e., 3/4 of 40 days) are not incorporated. Periodicities that are of most interest are those related to the solar rotation variation near 25-35 days. The first and second sub-harmonics of the solar rotation variation around 8-12 days and 13-18 days are also included with this treatment of the data. Meanwhile, longer-period variability (e.g., solar cycle and sea-

sonal effects and those due to Mars’ orbital eccentricity) along with short-term variability (e.g., disturbances from the lower and middle atmosphere) are largely eliminated. Solar flare days (M5 GOES class flares or greater) are considered data gaps to minimize additional disturbances not related to the solar rotation in flux.

Correlation analyses are performed using the Python package ‘`scipy.stats.linregress`’ and include the standard error (SE) of the regression slope. SE is defined as

$$SE = \sqrt{\frac{1}{(n-2)} \frac{\sum_0^i (y_i - \hat{y}_i)^2}{\sum_0^i (x_i - \bar{x})^2}} \quad (1)$$

where n is the total sample size, y_i is the actual value of the response variable, \hat{y}_i is the predicted value of the response variable, x_i is the actual value of the predictor variable, and \bar{x} is the mean value of the predictor variable. The smaller the SE, the lower the variability around the coefficient estimate for the regression slope. For all cases examined with $r > 0.5$, SE values are found to be $< 20\%$ of the slope providing confidence in the statistical results herein presented. Note that the focus of this work is on the solar rotation variation as a tracer of short-term solar-driven impacts on thermospheric density. Thus only periods with $r > 0.5$ are used in computing estimates of slope values. Furthermore, only cases with $r > 0.5$ include SE values that are sufficiently small to provide confidence in the statistical results.

4 Correlation Analyses and Comparative Results

Figure 2 shows a direct comparison between the ‘simultaneous’ response of Earth’s and Mars’ thermospheric densities to ~ 7 prominent solar rotation variations in 121.6 nm flux from 11 September 2015 to 1 April 2016 under high solar flux conditions. This period is characterized by the largest and most persistent ~ 27 -day variations observed concurrently in Mars’ (Hughes et al., 2022) and Earth’s thermospheric densities from 28 November 2013 to 24 September 2021 (see also Figure 3a and related discussion). The 5-day running means of 40-day density and irradiance residuals (expressed as % relative changes, see Section 3) are shown in Figures 2a’-2b’ for Earth and Mars, respectively. The ~ 121.6 nm irradiance (scaled by a factor of 3) shows that ± 7 -10% variations in flux correspond to around ± 20 -30% variations in thermospheric density at Earth near 460 km and around ± 10 -25% variations in thermospheric density at Mars near 220 km. The scatter plots of mass density relative changes versus 121.6 nm irradiance relative changes for this ~ 7 -month period of prominent solar rotation forcing are contained in Figures 2a’’-2b’’ for Earth and Mars, respectively. The legends of Figures 2a’’-2b’’ include slopes (m) and correlation coefficients (r) from the fitting algorithm. (Note that in the following the terms ‘slopes’ and ‘sensitivities’ are used interchangeably). The noted m and r values of $\sim 2.63 \pm 0.24$ ($\sim 1.70 \pm 0.20$) and ~ 0.67 (~ 0.56) at Earth (Mars), respectively, indicate that the terrestrial response to the solar rotation in flux is significantly stronger than that at Mars for a similar density level (Table 1 and Figure 4 contain more quantitative analyses). This result confirms previous findings (e.g., Forbes et al., 2006, 2007; Keating and Bougher, 1987, 1992; Bougher et al., 1999, 2015, 2017; Thiemann and Dominique, 2021) reporting reduced sensitivities to solar irradiance for Mars’ thermosphere generally explained by the increased importance of CO_2 cooling in damping solar EUV energy at Mars. The lower correlation for Mars may be due to short-term density variability not associated with solar effects. A detailed investigation of possible impacts from the lower and middle atmosphere (e.g., waves and dust storm effects) and CO_2 cooling effects, outside the purview of the current study, is left for future investigations. Note that while shorter wavelength irradiance may be more representative of solar flux absorption in the middle and upper thermospheric regions, Figure 2 has the critical advantage of showing the ‘same’ Lyman- α band measured concurrently at the two planets. Furthermore, solar rotation variability at different wavelengths is expected to be strongly correlated.

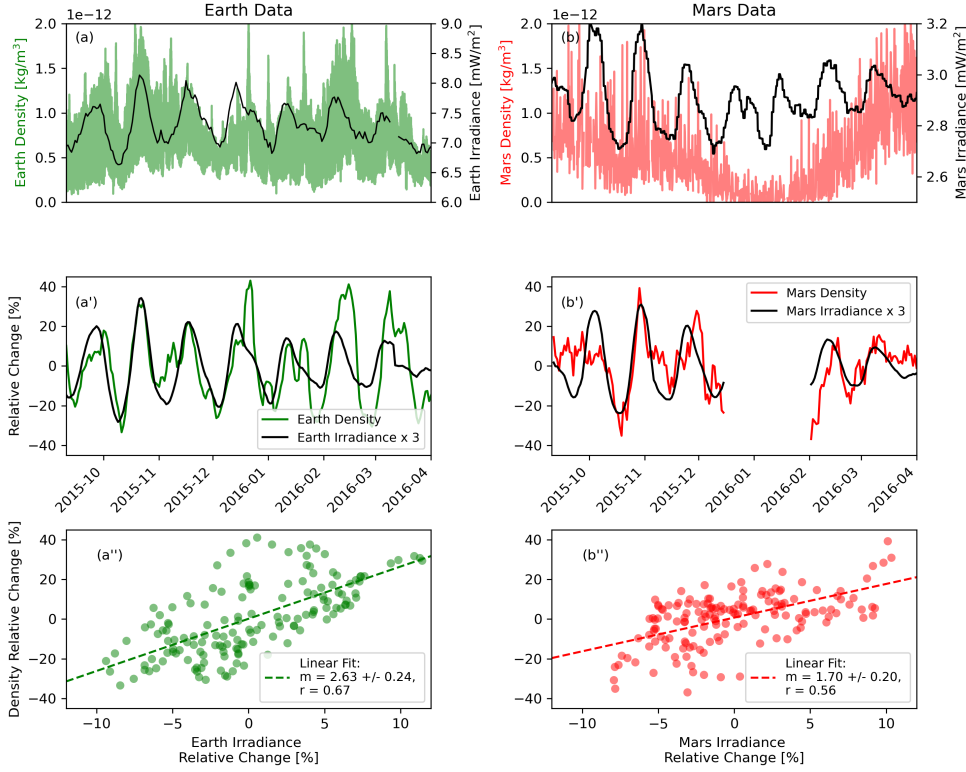


Figure 2. (a) Globally (i.e., $\pm 87^\circ$ latitude and $0\text{--}360^\circ$ longitude) averaged Swarm-C POD thermospheric density (green line) and GOES-15 121.6 nm irradiance (black line) from 11 September 2015 to 1 April 2016. (b) NGIMS total mass density near 220 km (red line) and EUVM 121.6 nm irradiance (black line) for the same time interval as (a). (a')–(b') 5-day running means of 40-day residuals of (a) and (b) expressed as % values. (a'') Scatter plot of Swarm-C density relative changes versus GOES irradiance relative changes (green dots) for the same time interval as (a) and (a'). (b'') Same as (a'') but for NGIMS density relative changes versus EUVM irradiance relative changes at Mars. The Pearson correlation coefficients (r), slopes (m), and fitting lines are also included. No data points for 15 December 2015 – 31 January 2016 (i.e., for $r < 0.5$, see gap in panel (b'')) are included in (a'') and (b''). For Mars, LT varies between $\sim 0.5\text{--}14.5\text{ hr}$, latitude changes from $\sim 47^\circ\text{S}$ to $\sim 56.2^\circ\text{N}$, and Ls varies between $\sim 39.5^\circ$ and $\sim 105.4^\circ$. The average solar radio flux at 10.7 cm (F10.7) measured at Earth is ~ 110 sfu.

A closer inspection of Figure 2 also reveals an apparent phase shift between the neutral density response to solar irradiance of both planetary thermospheres. Further analyses (not shown here) demonstrate this phase shift to correspond to approximately one terrestrial/Martian day. This lag in the density response to the solar rotation variation in flux may be an indication of the plausible timescale at play related to heating and is in excellent agreement with previous studies (e.g., Jacchia et al., 1973; Hedin and Mayr, 1987). Yet, it is important to note that our ability to accurately capture such small timescales is impacted by the data processing methods adopted. The correlation analyses are performed on 5-day running means of 40-day residuals. This 5-day averaging, which is used to highlight variability associated with the solar rotation variation by effectively minimizing short-term variability due to lower atmospheric forcing, challenges our ability to discern phase delays on such short timescales. Correlation analyses performed during other periods (e.g., Figure 3 near solar minimum) provide less conclusive results, sug-

gesting that further work in this direction is needed that may require dedicated modeling effort along with targeted correlative methods.

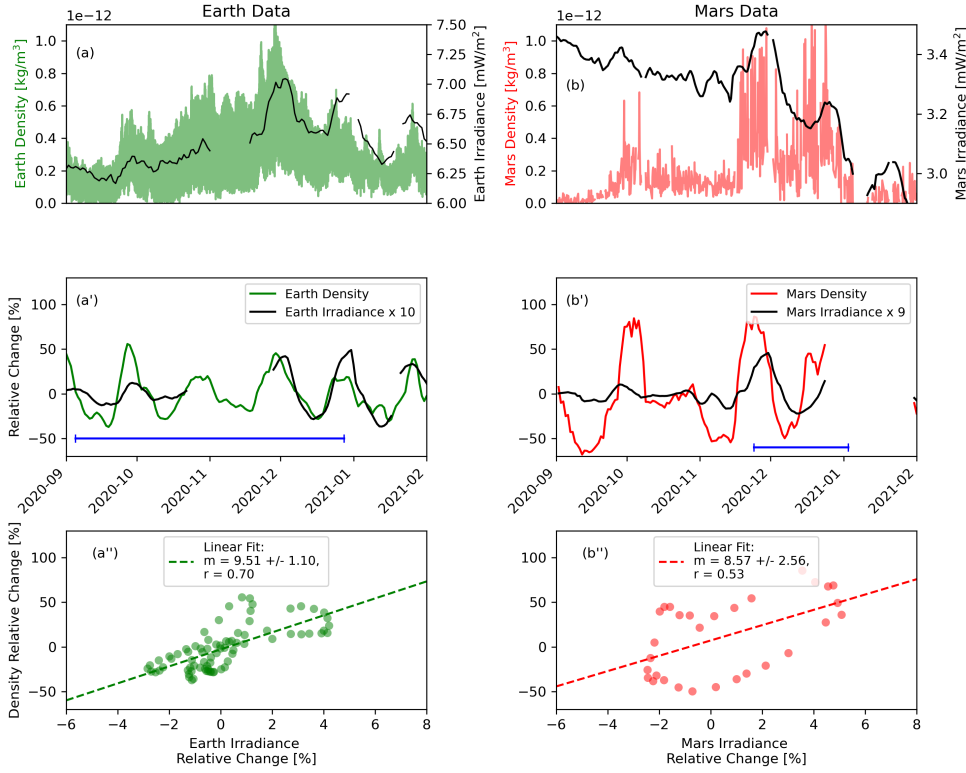


Figure 3. Same as Figure 2 but for the time period extending from September 2020 to January 2021 under low solar flux conditions (with an average F10.7 at Earth near 70 sfu). For Mars, LT varies between ~ 2.4 -hr and ~ 23.1 -hr, latitude changes from $\sim 66.1^\circ$ S to $\sim 74.2^\circ$ N, and Ls varies between $\sim 270.3^\circ$ and $\sim 350.2^\circ$. The NGIMS altitude is selected to be near 240 km to best conform with the average density values observed by Swarm-C during this period (Swarm-C's mean altitude decreased by about 20 km from 2015 to 2020, as shown in Figure 1b).

Figure 3 shows similar depictions to those contained in Figure 2 but is focused on a period extending from 6 September 2020 to 3 January 2021 with reduced solar flux conditions (F10.7 ~ 70 sfu versus ~ 110 sfu) and similar LT coverage by NGIMS. Large slopes are found for both planetary thermospheres, with values near 9.51 ± 1.10 and 8.57 ± 2.56 for Earth and Mars, respectively. In agreement with the 2015 case, the terrestrial response to the solar rotation in flux is stronger (by about 10-20%) than that of Mars for a similar density level. Comparisons between Figures 2 and 3 reveal a significantly increased response (by a factor upwards of 5) of the middle thermospheric densities to the solar rotation in flux during the late-2020 period. A higher response during solar low conditions is not unexpected as shown empirically by Hedin and Mayr (1987) in the context of terrestrial exospheric temperature dependencies on F10.7 (see Figure 6). While EUV forcing decreases at solar minimum, adiabatic cooling due to rising motions in global circulation plays a progressively more important role in the heat budget as solar activity increases. For higher levels of solar EUV flux, strong vertical winds and adiabatic cooling suppress the density response on the dayside at low to middle latitudes (Bougher et al., 1999, 2000, 2009, 2015).

It should be noted that the 2015 period in Figure 2 is near aphelion while the 2020 period in Figure 3 is close to perihelion. Thus some seasonal dependencies that may lead to a stronger response during the late-2020 period compared with the late-2015/early-2016 period may not be completely excluded. Nevertheless, correlation analyses performed during other correlative periods under solar low conditions during 2018-2019 demonstrate analog increased slopes supporting our conclusion that decreased solar flux level is likely the principal contributor to the increased slopes observed during 2020. The authors also note that the slope for both planets is influenced by the time ranges chosen. For Earth, a window that includes all of the January 2021 peak results in a lower slope, and a window that includes more of the October 2020 peak results in a higher slope. For Mars, shifting the window to earlier times results in an increased slope. For both planets, the signal in the 2020 period is weaker, and our estimates of the slope are less accurate, as the availability of concurrent solar rotation variations is limited to 2-3 rotations. Thus follow on comprehensive observational studies and targeted modeling efforts focused on quantifying the solar cycle dependency on the thermospheric response to the solar rotation variation are needed to fully characterize this dependency and understand connections to heating and cooling rates/efficiencies, as noted by previous work by Richards, 2012.

Table 1 summarizes the correlation results (reported as slope values and uncertainties in units of % density over % irradiance) between NGIMS total mass density and EUVM 0-7 nm, 17-22 nm, 0-45 nm, and 121.6 nm irradiances at ~ 200 km, ~ 220 km, and ~ 240 km altitude and between Swarm-C total mass density and GOES-15 121.6 nm irradiance with all density data combined, and restricting to daytime, nighttime, latitudes $>45^\circ$, and latitudes $<45^\circ$. Shown are three cases (from the top): (a) all the periods with $r \geq 0.5$ during 2015-2021, (b) the 10 September 2015 - 1 April 2016 period, and (c) the 1 September 2020 - 31 January 2021 period. The data are separated by altitude, day, night, and latitude before generating the relative changes used in the fitting routine. As previously discussed, important irradiance and altitude differences in the density response to the solar rotation variation are found for all cases examined. For Mars, for cases a and b, the 121.6 nm irradiance is found to have higher slopes ($m \simeq 2.6$ -5.1 depending on altitude) compared to the other three bands (~ 0.4 -1.6), while all irradiances exhibit higher slopes at ~ 240 km compared to 200 km). The higher slope values for the Lyman- α case can be explained by weaker solar rotation variability in Lyman- α , i.e., while the density change is the same for all channels, the irradiance change is the smallest for Lyman- α . In agreement with the terrestrial results by Guo et al. (2007), m and r are characterized by small dependencies on latitude and between daytime ($m \simeq 3.56 \pm 0.33$) and nighttime ($m \simeq 3.74 \pm 0.36$) conditions. Wind resulting from heating can impact day-night circulation changing temperature and composition that in turn changes neutral density (e.g., Qian et al., 2011), yet our results indicate that day/night differences in the sensitivities at Earth may be $<5\%$ for all solar flux conditions examined. Note that MAVEN's orbital characteristics and the limited number of correlative events make it challenging to reliably quantify day/night, and latitude dependencies at Mars.

The median sensitivities as a function of altitude during the September 2015 - April 2016 and September 2020 - January 2021 periods are contained in Figures 4a and 4b, respectively. Earth's slope values at Mars' 'equivalent' heights of ~ 220 km and ~ 240 km are also shown. During the late-2015/early-2016 period, Mars' thermospheric slope increases with altitude up to ~ 175 km, is relatively altitude-independent between ~ 180 km and ~ 220 km (with m values of ~ 1.8), increases significantly between ~ 220 km and ~ 240 km (to m values up to ~ 2.2). During the late-2020 period, Mars' thermospheric slope is relatively constant between ~ 205 and ~ 220 (with m values near 12.5) and then shows a prominent decrease up to ~ 240 km before increasing again between ~ 240 -260 km. The growth of slopes with altitude below ~ 240 km in Figure 4a and ~ 220 km in Figure 4b may be explained by increased efficiency in energy deposition (similar to previous terrestrial studies, e.g., Richards, 2012; Thiemann et al., 2017a). This increase is

Table 1. List of slope values (as % density over % irradiance) obtained applying correlation analyses to relative changes of NGIMS, EUVM, Swarm-C, and GOES-16 data as an average of all the periods with $r \geq 0.5$ during 2015-2021 (top), during September 2015 - April 2016 (middle), and during September 2020 - January 2021 (bottom). Shown are slopes from correlation analysis between NGIMS total mass density and EUVM 0-7 nm, 17-22 nm, 0-45 nm, and 121.6 nm irradiances at ~ 200 km, ~ 220 km, and ~ 240 km; and slopes from correlation analysis between Swarm-C in situ total mass density and GOES-15 121.6 nm irradiance combining all density data, during daytime ($6 \leq LT < 18$), during nighttime ($LT < 6$ or ≥ 18), for latitudes poleward of $\pm 45^\circ$, and (e) for latitudes equatorward of $\pm 45^\circ$. The Pearson correlation coefficient (r) is > 0.5 for all cases/altitudes/periods.

Sensitivity

All $r > 0.5$

<i>Mars, Altitude</i>	0-7 nm	17-22 nm	0-45 nm	121.6 nm
200 km	0.37 ± 0.05	1.37 ± 0.19	1.12 ± 0.15	2.59 ± 0.48
220 km	0.55 ± 0.10	1.84 ± 0.30	1.45 ± 0.24	5.05 ± 1.05
240 km	0.78 ± 0.13	1.95 ± 0.34	1.63 ± 0.28	3.93 ± 0.81
<i>Earth, Case</i>	121.6 nm			
All	3.75 ± 0.38			
Day	3.56 ± 0.33			
Night	3.74 ± 0.36			
Lat $> \pm 45^\circ$	3.82 ± 0.37			
Lat $\leq \pm 45^\circ$	3.69 ± 0.37			

High Solar Flux (2015-2016)

<i>Mars, Altitude</i>	0-7 nm	17-22 nm	0-45 nm	121.6 nm
200 km	0.32 ± 0.04	0.68 ± 0.08	0.63 ± 0.07	1.75 ± 0.17
220 km	0.31 ± 0.04	0.67 ± 0.10	0.62 ± 0.09	1.70 ± 0.20
240 km	0.38 ± 0.06	0.80 ± 0.13	0.73 ± 0.11	1.97 ± 0.27
<i>Earth, Case</i>	121.6 nm			
All	2.63 ± 0.24			
Day	2.93 ± 0.23			
Night	2.19 ± 0.29			
Lat $> \pm 45^\circ$	2.56 ± 0.25			
Lat $\leq \pm 45^\circ$	2.69 ± 0.23			

Low Solar Flux (2021-2022)

<i>Mars, Altitude</i>	0-7 nm	17-22 nm	0-45 nm	121.6 nm
200 km	1.56 ± 0.14	7.66 ± 0.66	6.3 ± 0.55	13.1 ± 1.28
220 km	1.57 ± 0.25	7.91 ± 1.17	6.46 ± 0.98	12.91 ± 2.26
240 km	1.08 ± 0.29	5.66 ± 1.36	4.57 ± 1.14	8.57 ± 2.56
<i>Earth, Case</i>	121.6 nm			
All	9.51 ± 1.10			
Day	7.20 ± 0.61			
Night	7.83 ± 0.77			
Lat $> \pm 45^\circ$	9.42 ± 1.13			
Lat $\leq \pm 45^\circ$	9.60 ± 1.08			

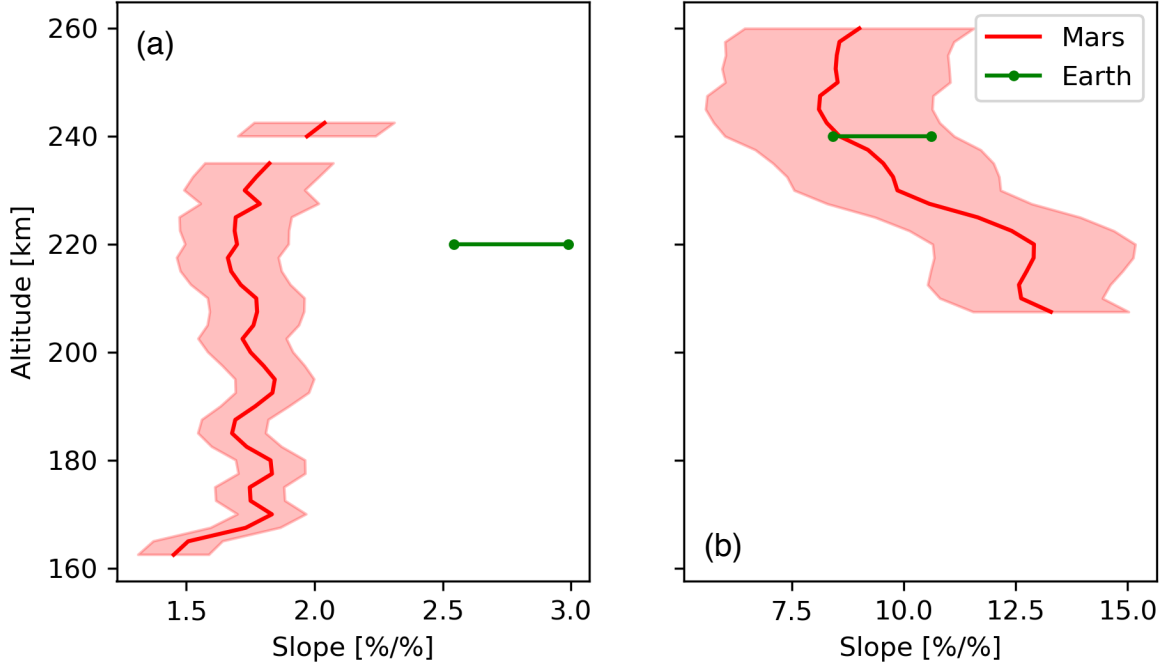


Figure 4. (a) Sensitivity of thermospheric total mass densities to the 121.6 nm irradiance at Mars (vertical red line) and Earth (horizontal green line) during the September 2015 - April 2016 period shown in Figure 2. (b) Same as (a), but for the September 2020 - January 2021 period shown in Figure 3. Earth’s slope values at Mars’ ‘equivalent’ heights of ~ 220 km and ~ 240 km are shown in (a) and (b), respectively. Uncertainties from the SE analysis are shown as shaded colors (horizontal lines) for Mars (Earth).

in general agreement with the results contained in Hughes et al. (2022) and is of similar magnitude to the local and nonlocal heating efficiency peaks in Gu et al. (2020) (see Figure 9). The slope increase with altitude is also consistent with the terrestrial study by Thiemann et al. (2017a), while the altitude dependency in the response is a possible consequence of changes in local time (LT) and season. Using revised EUV heating efficiencies, these authors attributed the sustained increase of sensitivities with altitude as evidence of larger EUV heating efficiency at higher heights. Gu et al. (2020) seem not to account for this thermal electron collision pathway for neutral heating, thus their heating efficiencies at high altitudes may be underestimated. Important to note that Thiemann et al. (2017a) show no clear high-altitude region of enhanced sensitivities. The decrease in the slope for the late-2020 case above about ~ 225 km (near the exobase, e.g., Chaffin et al., 2015) may be due to additional complexities potentially introduced by solar wind variability near or above the exobase (e.g., Hughes et al, 2022). Unfortunately, NGIMS provides no density measurements below about 200 km during the late-2020 period as a result of MAVEN’s periapsis orbit raise (see discussion in Section 2) and no $r > 0.5$ slopes are available for the late-2015/early-2016 period above ~ 250 . Yet, results in Figure 4b indicate a decrease in the slopes above about 220 km which is similar to the 2015 results above ~ 245 km (not shown). Note that SE estimates in the correlation analyses are within 20% even in the 220-260 km altitude range, providing confidence in the robustness of the statistical analyses even at the upper heights. Note that the marked altitude gradient in the slopes near 220-240 is statistically significant during both 2015 and 2020, and when combining all periods with $r > 0.5$ (see Table 1). Furthermore, this result is consistent with the results of Hughes et al. (2022). As noted above, more com-

prehensive terrestrial and Martian observations with improved spatial and temporal coverage, along with targeted modeling efforts, are needed to better characterize the sensitivity of thermospheric density to short-term solar variability (including dependencies on altitude, LT, season, solar flux level, species, and irradiance band) and their associated differences in heating and cooling processes.

5 Summary and Conclusions

This paper investigated the comparative responses of Mars' and Earth's thermospheric total mass densities to the solar rotation variation in EUV flux by employing concurrent in situ MAVEN NGIMS and EUVM, Swarm-C POD, and GOES observations from late 2014 during solar maximum through mid-2021 near solar minimum. Correlation analyses revealed a prominent response of both planetary thermospheres to the ~ 27 -day variation in flux and large altitude dependencies in the thermospheric response at Mars. Consistent with our understanding of the increased importance of CO_2 cooling in damping solar EUV energy at Mars, Earth's daytime thermospheric density sensitivity to flux is found to be ~ 10 -50% larger than that of Mars for a similar density level. This result is in excellent agreement with earlier studies (e.g., Forbes et al. 2006) and the recent work by Thiemann and Dominique (2021) that showed Mars' exospheric EUV temperature sensitivities to be about 0.47 as sensitive to EUV variability as those at Earth. Similar to previous Martian (e.g., Hughes et al., 2022) and terrestrial (e.g., Thiemann et al., 2017a) studies, Mars' thermospheric density response to EUV forcing is shown to increase with altitude up to ~ 240 km (with m values up to $\simeq 2.8\%/%$). The slope's growth with altitude is interpreted as evidence that the EUV heating efficiency increases moving from the lower to the middle thermosphere, likely as a result of thermal electron heating of neutrals at high altitudes (Richards, 2012). The large slope increase between about 220 km and 240 km altitude is generally consistent with the results in Hughes et al. (2022) and closely resembles the local and nonlocal heating efficiency results in Gu et al. (2020). For Earth, the density response to the solar rotation variation in flux is found to vary only by up to $\sim 5\%$ between day and night and for different latitude sectors.

Correlative analyses and comparisons of Earth's and Mars' thermospheric density responses to the solar rotation variation in 4 flux bands near 0-7 nm, 17-22 nm, 0-45 nm, and 121.6 nm during 2015-2021 revealed notable effects likely associated with the solar cycle. A detailed study of two periods with prominent solar rotation variability during late-2015/early-2016 and late-2020 shows greatly increased sensitivities under reduced solar flux levels for both planetary thermospheres. Furthermore, a closer inspection of the late-2015/early-2016 period reveals an apparent phase shift corresponding to approximately one terrestrial/Martian day between the neutral density response to solar irradiance of both planetary thermospheres. While this time lag may be an indication of the timescale at play related to heating, the correlation technique adopted was shown to be inadequate to accurately capture the small timescales involved.

The responses of both thermospheres to solar irradiance are known to be largely driven by the absorption of solar EUV photons and by the efficiency of energy redistribution and dissipation. It is suggested that while the processes that shape Mars' thermospheric density response to solar rotation variability in flux are similar to those at Earth, some differences exist. The results herein contained provide important observational insights into processes relevant to the interpretation of the sources of short-term density variability in Mars' and Earth's thermospheres associated with solar drivers, and possible influences associated with the solar activity level. This study also indicates that further work focused on investigating differences between the terrestrial and Martian responses to heating and cooling processes under different solar flux conditions is needed. This effort is likely to require targeting modeling work to complement dedicated data-oriented studies.

6 Data Availability Statement

The NGIMS Level 2 version 8 density data (Benna and Lyness, 2014) are publicly available at <https://doi.org/10.17189/1518931>. The EUVM Level 3 version 1 daily irradiance data (Epavier 2022) are publicly available at <https://doi.org/10.17189/1517691>. Swarm-C POD-derived densities (Van Den LJssel et al., 2020) can be website: <https://earth.esa.int/eogateway/missions/swarm/data>. GOES irradiances can be accessed at <https://www.ngdc.noaa.gov/stp/satellite/goes/>.

Acknowledgments

FG and JH acknowledge support from the NASA Mars Data Analysis (MDAP) grant 80NSSC21K1821 to Orion Space Solutions. ET was supported by NASA MDAP grant 80NSSC20K0941 to the University of Colorado.

References

- M. Benna, E. Lyness (2014), MAVEN Neutral Gas and Ion Mass Spectrometer Data, NASA Planetary Data System, doi:10.17189/1518931
- Bougher, S. W. (1995), Comparative thermospheres: Venus and Mars, *Adv. in Sp. Res.*, 15(4), 21-45, doi:10.1016/0273-1177(94)00062-6
- Bougher, S. W., Engel, S., Roble, R. G., and Foster, B. (1999), Comparative terrestrial planet thermospheres: 2. Solar cycle variation of global structure and winds at equinox, *J. Geophys. Res.*, 104(E7), 16,591-16,611, doi:10.1029/1998JE001019
- Bougher, S. W., Engel, S., Roble, R. G., and Foster, B. (2000), Comparative terrestrial planet thermospheres: 3. Solar cycle variation of global structure and winds at solstices, *J. Geophys. Res.*, 105(E7), 17669-17692, doi:10.1029/1999JE001232
- Bougher, S. W., T. M. McDunn, K. A. Zoldak, and J. M. Forbes (2009), Solar cycle variability of Mars dayside exospheric temperatures: Model evaluation of underlying thermal balances, *Geophys. Res. Lett.*, 36, L05201, doi:10.1029/2008GL036376.
- Bougher, S., D. Pawlowski, J. Bell, S. Nelli, T. McDunn, J. Murphy, M. Chizek, and A. Ridley (2015), Mars Global Ionosphere-Thermosphere Model: Solar cycle, seasonal, and diurnal variations of the Mars upper atmosphere, *J. Geophys. Res. Planets*, 120, 311-342, doi:10.1002/2014JE004715.
- Bougher, S. W., Roeten, K. J., Olsen, K., Mahaffy, P. R., Benna, M., Elrod, M., ... and Jakosky, B. M. (2017). The structure and variability of Mars dayside thermosphere from MAVEN NGIMS and IUVS measurements: Seasonal and solar activity trends in scale heights and temperatures. *Journal of Geophysical Research: Space Physics*, 122(1), 1296-1313.
- Chaffin, M. S., Chaufray, J. Y., Deighan, J., Schneider, N. M., McClintock, W. E., Stewart, A. I. F., et al., (2015). Three-dimensional structure in the Mars H corona revealed by IUVS on MAVEN. *Geophysical Research Letters*, 42(21), 9001-9008.
- Chamberlin, P. C., T. N. Woods, and F. G. Eparvier (2007), Flare irradiance spectral model (FISM): Daily component algorithms and results, *Space Weather*, 5(7), S07005.
- Chamberlin, P. C., Woods, T. N., and Eparvier, F. G. (2008), Flare Irradiance Spectral Model (FISM): Flare component algorithms and results, *Space Weather*, 6, S05001, doi:10.1029/2007SW000372.
- Dickinson, R. E., Ridley, E. C., and Roble, R. G. (1981), A three-dimensional general circulation model of the thermosphere, *J. Geophys. Res.*, 86(A3), 1499-1512, doi:10.1029/JA086iA03p01499.

- Elrod, M. K., Curry, S. M., Thiemann, E. M. B., and Jain, S. K. (2018). September 2017 solar flare event: Rapid heating of the Martian neutral upper atmosphere from the X-class flare as observed by MAVEN. *Geophysical Research Letters*, 45, 8803– 8810. <https://doi.org/10.1029/2018GL077729>
- England, S. L., et al. (2016), Simultaneous observations of atmospheric tides from combined in situ and remote observations at Mars from the MAVEN spacecraft, *J. Geophys. Res. Planets*, 121, 594-607, doi:10.1002/2016JE004997.
- England, S. L., Liu, G., Yigit, E., Mahaffy, P. R., Elrod, M., Benna, M., Nakagawa, H., Terada, N., and Jakosky, B. (2017), MAVEN NGIMS observations of atmospheric gravity waves in the Martian thermosphere, *J. Geophys. Res. Space Physics*, 122, 2310– 2335, doi:10.1002/2016JA023475.
- England, S. L., Liu, G., Kumar, A., Mahaffy, P. R., Elrod, M., Benna, M., et al. (2019), Atmospheric tides at high latitudes in the Martian upper atmosphere observed by MAVEN and MRO, *J. Geophys. Res. Space Physics*, 124, doi:10.1029/2019JA026601.
- Eparvier, F. G., Chamberlin, P. C., Woods, T. N., and Thiemann, E. M. B. (2015), The solar extreme ultraviolet monitor for MAVEN, *Space Science Reviews*, 195(1-4), 293-301.
- Epavier (2022), MAVEN EUV Modelled Data Bundle, NASA Planetary Data System, doi.org/10.17189/1517691
- Eparvier, F. G., D. Crotser, A. R. Jones, W. E. McClintock, M. Snow, and T. N. Woods, The Extreme Ultraviolet Sensor (EUVS) for GOES-R, *Proc. SPIE* 7438, *Solar Physics and Space Weather Instrumentation III*, 743804 (September 23, 2009). doi:10.1117/12.826445.
- Fan, Y. (2009), Y. Magnetic Fields in the Solar Convection Zone, *Living Rev. Sol. Phys.* 6, 4, doi:10.12942/lrsp-2009-4.
- Fan, Y. (2021), Magnetic fields in the solar convection zone. *Living Reviews in Solar Physics*, 18(1), 1-96.
- Fang, X., Pawlowski, D., Ma, Y., Bougher, S., Thiemann, E., Eparvier, F., et al. (2019). Mars upper atmospheric responses to the 10 September 2017 solar flare: A global, time-dependent simulation. *Geophysical Research Letters*, 46, 9334– 9343. <https://doi.org/10.1029/2019GL084515>
- Fang, X., Forbes, J. M., Benna, M., Montabone, L., Curry, S., and Jakosky, B. (2022). The origins of long-term variability in Martian upper atmospheric densities. *Journal of Geophysical Research: Space Physics*, 127, e2021JA030145. <https://doi.org/10.1029/2021JA030145>
- Forbes, J. M., S. Bruinsma, and F. G. Lemoine (2006), Solar rotation effects on the thermospheres of Mars and Earth, *Science*, 312, 1366-1368, doi:10.1126/science.1126389.
- Forbes, J. M. (2007). Dynamics of the thermosphere. *Journal of the Meteorological Society of Japan. Ser. II*, 85, 193-213.
- Forbes, J. M., S. Bruinsma, F. G. Lemoine, B. R. Bowman, and A. Konopliv (2007), Satellite drag variability at Earth, Mars, and Venus due to solar rotation, *J. Spacecr. Rockets*, 44(6), 1160– 1164, doi:10.2514/1.28013.
- Forbes, J. M., F. G. Lemoine, S. L. Bruinsma, M. D. Smith, and X. Zhang (2008), Solar flux variability of Mars’ exosphere densities and temperatures, *Geophys. Res. Lett.*, 35, L01201, doi:10.1029/2007GL031904.
- Friis-Christensen, E., H. Lühr, D. Knudsen, and R. Haagmans (2008), Swarm- An earth observation mission investigating geospace, *Adv. Space Res.*, 41(1), 210– 216.
- Gasparini, F., Forbes, J. M., Doornbos, E. N., and Bruinsma, S. L. (2015), Wave coupling between the lower and middle thermosphere as viewed from TIMED and GOCE, *J. Geophys. Res. Space Physics*, 120, 5788-5804, doi:10.1002/2015JA021300.

- Gasperini, F., Hagan, M. E., and Forbes, J. M. (2018), Seminal evidence of a 2.5-sol ultra-fast Kelvin wave in Mars' middle and upper atmosphere, *Geophys. Res. Lett.*, 45, 6324-6333, doi:10.1029/2018GL077882.
- Gasperini, F., Liu, H., and McInerney, J. (2020), Preliminary evidence of Madden-Julian Oscillation effects on ultrafast tropical waves in the thermosphere, *J. Geophys. Res. Space Physics*, 125, e2019JA027649, doi:10.1029/2019JA027649.
- Girazian, Z., Mahaffy, P., Lee, Y., and Thiemann, E. M. B. (2019), Seasonal, solar zenith angle, and solar flux variations of O+ in the topside ionosphere of Mars, *J. Geophys. Res. Space Physics*, 124, 3125-3138, doi:10.1029/2018JA026086.
- González-Galindo, F., López-Valverde, M. A., Forget, F., García-Comas, M., Millour, E., and Montabone, L. (2015). Variability of the Martian thermosphere during eight Martian years as simulated by a ground-to-exosphere global circulation model, *J. Geophys. Res. Planets*, 120, 2020-2035, doi:10.1002/2015JE004925.
- Guo, J., W. Wan, J. M. Forbes, E. Sutton, R. S. Nerem, T. N. Woods, S. Bruinsma, and L. Liu (2007), Effects of solar variability on thermosphere density from CHAMP accelerometer data, *J. Geophys. Res.*, 112, A10308, doi:10.1029/2007JA012409.
- Gu, H., Cui, J., Niu, D. D., Cao, Y. T., Wu, X. S., Li, J., ... and Wei, Y. (2020). Neutral heating efficiency in the dayside Martian upper atmosphere. *The Astronomical Journal*, 159(2), 39.
- Hagan, M. E., and Oliver, W. L. (1985). Solar cycle variability of exospheric temperature at Millstone Hill between 1970 and 1980. *Journal of Geophysical Research: Space Physics*, 90(A12), 12265-12270.
- Hedin, A. E., and Mayr, H. G. (1987), Solar EUV induced variations in the thermosphere, *J. Geophys. Res.*, 92(D1), 869-875, doi:10.1029/JD092iD01p00869.
- Hughes, J., Gasperini, F., and Forbes, J. M. (2022). Solar rotation effects in Martian thermospheric density as revealed by five years of MAVEN observations, *J. Geophys. Res. Planets*, 127, e2021JE007036. <https://doi.org/10.1029/2021JE007036>
- Jacchia, L. G., J. W. Slowey, and I. G. Campbell (1973), An analysis of the solar-activity effects in the upper atmosphere, *Planet. Space*, 21, 1835-1842.
- Jakosky, B.M., Lin, R.P., Grebowsky, J.M. et al. The Mars Atmosphere and Volatile Evolution (MAVEN) Mission. *Space Sci Rev* 195, 3–48 (2015). <https://doi.org/10.1007/s11214-015-0139-x>
- Keating, G. M., and S. W. Bougher (1987), Neutral upper atmospheres of Venus and Mars, *Adv. Space Res.*, 7(12), 57– 71.
- Keating, G. M., and S. W. Bougher (1992), Isolation of major Venus thermospheric cooling mechanism and implications for Earth and Mars, *J. Geophys. Res.*, 97(A4), 4189– 4197.
- Lean, J. (1997), The Sun's variable radiation and its relevance for Earth 1, *Ann. Rev. Astron. Astrophys.*, 35(1), 33-67.
- Liu, G., S. England, R. J. Lillis, P. R. Mahaffy, M. Elrod, M. Benna, and B. Jakosky (2017), Longitudinal structures in Mars' upper atmosphere as observed by MAVEN/NGIMS, *J. Geophys. Res.*, 122, 1258-1268, doi:10.1002/2016JA023455.
- Luo, P., S. Jin, and Q. Shi (2022), Undifferenced Kinematic Precise Orbit Determination of Swarm and GRACE-FO Satellites from GNSS Observations. *Sensors*, 22, 1071, doi:10.3390/s22031071.
- Machol, J., Snow, M., Woodraska, D., Woods, T., Viereck, R., and Coddington, O. (2019). An improved lyman-alpha composite. *Earth and Space Science*, <https://doi.org/10.1029/MACHOL ET AL.2019EA000648>
- Mahaffy, P. R., et al. (2014), The neutral gas and ion mass spectrometer on the Mars Atmosphere and Volatile Evolution Mission, *Space Sci. Rev.*, 185, doi:10.1007/s11214-11014-10091-11211.

- Mahaffy, P. R., M. Benna, M. Elrod, R. V. Yelle, S. W. Bougher, S. W. Stone, and B. M. Jakosky (2015), Structure and composition of the neutral upper atmosphere of Mars from the MAVEN NGIMS investigation, *Geophys. Res. Lett.*, 42, 8951-8957, doi:10.1002/2015GL065329.
- McClintock, W. E., Rottman, G. J., and Woods, T. N. (2005). Solar-Stellar Irradiance Comparison Experiment II (Solstice II): Instrument concept and design. *Solar Physics*, 230, 225–258. <https://doi.org/10.1007/s11207-005-7432-x>
- McClintock, W. E., Snow, M., and Woods, T. N. (2005). Solar-Stellar Irradiance Comparison Experiment II (SOLSTICE II): Pre-launch and on-orbit calibrations. *Solar Physics*, 230, 259–294. <https://doi.org/10.1007/s11207-005-1585-5>
- Richards, P. G. (2012). Re-evaluation of thermosphere heating by solar EUV and UV radiation. *Canadian Journal of Physics*, 90(8), 759-767.
- Roble, R. G., Ridley, E. C., and Dickinson, R. E. (1987), On the global mean structure of the thermosphere, *J. Geophys. Res.*, 92(A8), 8745– 8758, doi:10.1029/JA092iA08p08745.
- Siemes, C., de Teixeira da Encarnação, J., Doornbos, E., van den IJssel, J., Kraus, J., Peresty, R., et al. (2016). Swarm accelerometer data processing from raw accelerations to thermospheric neutral densities. *Earth, Planets and Space*, 68(1), 92.
- Solomon, S. C., and Qian, L. (2005), Solar extreme-ultraviolet irradiance for general circulation models. *J. Geophys. Res.* 110. doi:10.1029/2005JA011160.
- Snow, M., McClintock, W. E., Rottman, G., and Woods, T. N. (2005). Solar-Stellar Irradiance Comparison Experiment II (SOLSTICE II): Examination of the solar-stellar comparison techniques. *Solar Physics*, 230, 295–324. <https://doi.org/10.1007/s11207-005-8763-3>
- Snow, M., W. E. McClintock, D. Crotser and F. G. Eparvier (2009), EUVS-C: the measurement of the magnesium II index for GOES-R EXIS”, *Proc. SPIE 7438, Solar Physics and Space Weather Instrumentation III*, 743803. doi:10.1117/12.828566.
- Stone, S. W., Yelle, R. V., Benna, M., Elrod, M. K., and Mahaffy, P. R. (2018). Thermal structure of the Martian upper atmosphere from MAVEN NGIMS. *Journal of Geophysical Research: Planets*, 123(11), 2842-2867.
- Terada, N., et al. (2017), Global distribution and parameter dependences of gravity wave activity in the Martian upper thermosphere derived from MAVEN/NGIMS observations, *J. Geophys. Res. Space Physics*, 122, 2374–2397, doi:10.1002/2016JA023476.
- Thiemann, E. (2016), Multi-spectral sensor driven solar EUV irradiance models with improved spectro-temporal resolution for space weather applications at Earth and Mars, PhD thesis, Univ. of Colorado, Boulder, Colo.
- Thiemann, E. M. B., Dominique, M., Pilinski, M. D., and Eparvier, F. G. (2017a), Vertical thermospheric density profiles from EUV solar Occultations made by PROBA2 LYRA for solar cycle 24. *Space Weather*, 15, 1649–1660
- Thiemann, E. M. B., P. C. Chamberlin, F. G. Eparvier, B. Templeman, T. N. Woods, S. W. Bougher, B. M. Jakosky (2017b), The MAVEN EUVM model of solar spectral irradiance variability at Mars: Algorithms and results, *J. Geophys. Res. Space Physics*, 122, 2748-2767, doi:10.1002/2016JA023512.
- Thiemann, E. M. B., Eparvier, F. G., Bougher, S. W., Dominique, M., Anderson, L., Girazian, Z., et al. (2018). Mars thermospheric variability revealed by MAVEN EUVM solar occultations: Structure at aphelion and perihelion and response to EUV forcing. *Journal of Geophysical Research: Planets*, 123, 2248–2269. <https://doi.org/10.1029/2018JE005550>
- Thiemann, E. M. B., Eparvier, F. G., Woodraska, D., Chamberlin, P. C., Machol, J., Eden, T., et al. (2019), The GOES-R EUVS model for EUV irradiance variability, *Journal of Space Weather and Space Climate*, 9, A43.

- Thiemann, E. M., and Dominique, M. (2021), PROBA2 LYRA Occultations: Thermospheric Temperature and Composition, Sensitivity to EUV Forcing, and Comparisons With Mars. *Journal of Geophysical Research: Space Physics*, 126(7), e2021JA029262.
- Van Den Ljssel, J., B. Forte, and O. Montenbruck (2016), Impact of Swarm GPS receiver updates on POD performance, *Earth Planets Space*, 68– 85, doi:10.1186/s40623-016-0459-4.
- Van Den Ljssel, J., Doornbos, E., Iorfida, E., March, G., Siemes, C., & Montenbruck, O. (2020), Thermosphere densities derived from Swarm GPS observations, *Advances in Space Research*, 65(7), 1758-1771, doi:10.1016/j.asr.2020.01.004
- Viereck, R., F. Hanser, J. Wise, S. Guha, A. Jones, D. McMullin, S. Plunket, D. Strickland, and S. Evans (2007), Solar extreme ultraviolet irradiance observations from GOES: Design characteristics and initial performance, in *Proceedings of SPIE 6689, Solar Physics and Space Weather Instrumentation II*, pp. 66890K, SPIE, San Diego, Calif., doi:10.1117/12.734886.
- Visser, P., Doornbos, E., van den IJssel, J., and Da Encarnação, J. T. (2013). Thermospheric density and wind retrieval from Swarm observations. *Earth, Planets and Space*, 65(11), 12.
- Woods, T. N., & Rottman, G. J. (2002). Solar ultraviolet variability over time periods of aeronomic interest. *Geophysical Monograph-American Geophysical Union*, 130, 221-234.
- Yiğit, E., S. L. England, G. Liu, A. S. Medvedev, P. R. Mahaffy, T. Kuroda, and B. M. Jakosky (2015b), High-altitude gravity waves in the Martian thermosphere observed by MAVEN/NGIMS and modeled by a gravity wave scheme, *Geophys. Res. Lett.*, 42, 8993– 9000, doi:10.1002/2015GL065307.
- Yuan, L.L., Jin, S.G., Calabria, A., 2019. Distinct thermospheric mass density variations following the September 2017 geomagnetic storm from GRACE and Swarm. *J. Atmos. Sol. Terr. Phys.* 184, 30–36. <https://doi.org/10.1016/j.jastp.2019.01.007>.
- Zurek, R. W., R. A. Tolson, S. W. Bougher, R. A. Lugo, D. T. Baird, J. M. Bell, and B. M. Jakosky (2017), Mars thermosphere as seen in MAVEN accelerometer data, *J. Geophys. Res. Space Physics*, 122, 3798-3814, doi:10.1002/2016JA023641.